

<https://doi.org/10.1038/s43247-024-01347-1>

Ocean acidification offsets the effect of warming on sediment denitrification and associated nitrous oxide production

Check for updates

Michelle Nicole Simone ^{1,2}✉, Dirk Vincent Eler ², Kai Georg Schulz ², Joanne Margaret Oakes ² & Bradley David Eyre ²

Rates of denitrification and associated nitrous oxide (N₂O) production are expected to increase with global warming, leading to positive climate feedback. However, previous studies have not considered the combined effect of ocean acidification (OA, $p\text{CO}_2 \sim 900 \mu\text{atm}$) and warming on denitrification rates and N₂O production. Here we used a series of whole core incubation studies to assess the combined impact of warming and OA on estuarine sediment denitrification rates and N₂O production. Strong warming (+5 °C over mean in situ conditions) increased N₂O production by $\sim 4.2 \mu\text{mol-N m}^{-2} \text{d}^{-1}$ and denitrification by $\sim 43 \mu\text{mol-N m}^{-2} \text{d}^{-1}$, fuelled by water column nitrate (D_w), but decreased rates of nitrification-coupled denitrification in the sediment (D_n) by $\sim 82 \mu\text{mol-N m}^{-2} \text{d}^{-1}$. While D_n was not affected by OA, D_w decreased significantly by $51 \mu\text{mol-N m}^{-2} \text{d}^{-1}$ when OA was coupled with warmer temperatures. We estimate that OA may offset the increase in estuarine sediment denitrification and N₂O production expected from warming alone by up to 64% and reduce a potential positive climate feedback loop by inhibiting denitrification pathways.

Changes in the global nitrogen cycle have pushed the Earth's system outside the relatively stable state that had seen human civilisations arise¹. Anthropogenic rates of N₂ fixation, mostly due to industrialised forms of agriculture, now exceed natural biological fixation rates². Estuaries and coastal waters receive much of this anthropogenic nitrogen, where it stimulates the production of excess organic matter (eutrophication³). Nitrogen is permanently removed from the coastal zone via denitrification and anammox, which convert fixed nitrogen to di-nitrogen gas (N₂) that is ultimately lost to the atmosphere. Denitrification typically accounts for most of the N₂ produced in coastal sediments, with a widely reported ratio of 71:29 for denitrification:anammox⁴. This, in turn, acts as a control on ecosystem primary productivity⁵. However, denitrification also produces nitrous oxide (N₂O)⁶, a greenhouse gas with a global warming potential 296 times more than CO₂⁷.

In addition to excess nitrogen loading, increasing sea surface temperatures (SST) and ocean acidification (OA) are also impacting coastal ecosystems, with the cumulative effects increasing the risk of hypoxia potentially exacerbating the acidification of subsurface waters. The IPCC "high emissions" scenario projects a doubling of atmospheric CO₂ concentrations, reaching upwards of 1000 ppmv by the end of the century (RCP8.5⁸), resulting in increased global mean SST of $\sim 2\text{--}4 \text{ }^\circ\text{C}$ ⁹. The partial

pressure of CO₂ ($p\text{CO}_2$) in surface water will increase in line with atmospheric concentrations, leading to ocean acidification (OA), with increased concentrations of dissolved inorganic carbon (DIC), and a ~ 0.3 unit pH decrease¹⁰. Understanding how warming and OA will affect denitrification, and the associated production of N₂O is essential to assess the nitrogen removal capacity of the coastal zone, and the positive warming feedback loop from N₂O production in a high-CO₂ climate.

Warming increases potential dark denitrification up to an optimal temperature (T_{opt})^{11–13}. Potential dark denitrification rates may have a T_{opt} greater than anammox, suggesting that denitrification may become even more dominant as temperatures increase which, in turn, may increase the potential incomplete reduction and production of N₂O¹¹. However, warming was unlikely to directly affect the relative reduction of N by anammox or denitrification based on similar T_{opt} s for the two pathways in temperate estuarine sediments¹⁴. In contrast, OA effects on denitrification have not been widely investigated. In one study with high CO₂ concentrations and pH buffered to 7.2 there was an inverse relationship between CO₂ concentration and the rate of total N removal or denitrification efficiency, through the inhibition of denitrifying microbes' intracellular electron transport and consumption system¹⁵. Yet, despite both warming and OA having the potential to affect denitrification and N₂O production rates, both

¹Department of Environmental Science, Auckland University of Technology, Auckland 1010, New Zealand. ²Centre for Coastal Biogeochemistry, Faculty of Science and Engineering, Southern Cross University, Lismore, NSW 2480, Australia. ✉e-mail: Michelle.simone@aut.ac.nz; mnhsimone@gmail.com

individually and together, this combined effect has never been studied. Denitrifying and nitrifying gene abundance (16S rRNA genes, *amoA* and *nirS*) under individual and combined stressors of elevated temperatures ($\Delta+4^\circ\text{C}$) and CO_2 (750 ppm) have been investigated, with lower gene abundance in combined stressor treatments than at elevated temperatures under current CO_2 ¹⁶. A lower gene abundance may indicate that despite warming, OA could lead to a decrease in N_2 and N_2O production in a high- CO_2 climate, but no study has directly measured these N_2 and N_2O flux rates under these conditions. Here we evaluate how denitrification and N_2O production will be affected by a combination of increased temperature and $p\text{CO}_2$.

Through a series of whole core incubation studies, we were able to assess the combined impact of warming and OA on estuarine sediment denitrification rates and N_2O production. We found that OA may offset the warming increase in estuarine sediment denitrification and N_2O production by up to 64% and reduce a potential positive climate feedback loop by inhibiting denitrification pathways.

Results

Denitrification

Denitrification (D_{14}) rates were not significantly different between overlapping incubation controls in light and dark cycles (Supplementary Table 1) and thus were determined to be comparable and rates were left unadjusted. Supporting this, in situ, sediment characteristics were also unchanged across the two separate incubation times, with surface sediments C:N of 15.88 ± 1.34 , and $\delta^{13}\text{C}$ and $\delta^{15}\text{N}$ values of $\sim 22\text{‰}$ and 4.5‰ , respectively (error $<0.2\text{‰}$ for C:N and $\sim 1\text{‰}$ for $\delta^{13}\text{C}$ and $\delta^{15}\text{N}$ measured values).

There was a significant interacting effect of $p\text{CO}_2$ and temperature on denitrification rates ($F_{3,15} = 4.14$, $p = 0.025$), however this difference was only measurable at 28°C (Fig. 1a). For temperatures below 28°C , increasing temperature resulted in significant increases in D_{14} ($F_{3,8} = 22.03$, $p = 0.0003$; $F_{3,7} = 53.53$, $p < 0.0001$; for current and high $p\text{CO}_2$, respectively, Fig. 1a). Both $p\text{CO}_2$ conditions resulted in a decrease in net D_{14} at 28°C , but this decrease was significantly greater under high- $p\text{CO}_2$ ($F_{1,3} = 20.34$, $p = 0.02$). The $\sim 70\%$ decrease in net D_{14} under high- $p\text{CO}_2$ was a result of a decrease in light cycle net production that was 40% greater than the decrease under current- $p\text{CO}_2$ rates.

Greater insight into these differences was gained by the dissection of D_{14} into D_w and D_n . The D_{14} response was dominated by D_n across all treatments ($>50\%$ of total D_{14} , Fig. 1), except at 28°C under current- $p\text{CO}_2$, where D_n only accounted for 44% of D_{14} . However, there were no significant interactive effects of $p\text{CO}_2$ and temperature ($F_{3,16} = 2.68$, $p = 0.08$) and/or effect of $p\text{CO}_2$ on D_n production of N_2 ($F_{1,16} = 0.71$, $p = 0.41$). Differences in D_{14} production between $p\text{CO}_2$ conditions were therefore driven by an interactive effect of $p\text{CO}_2$ and temperature on D_w response ($F_{3,15} = 16.43$, $p < 0.0001$).

Under current- $p\text{CO}_2$, net D_w rates increased significantly with increased temperature ($F_{3,8} = 41.58$, $p < 0.0001$; Fig. 1d), with control rates ($38 \mu\text{mol-N m}^{-2} \text{d}^{-1}$) doubling in $\Delta+3^\circ\text{C}$ and $\Delta+5^\circ\text{C}$ cores (74 and $81 \mu\text{mol-N m}^{-2} \text{d}^{-1}$, respectively). In contrast, under high- $p\text{CO}_2$ D_w rates only increased at 26°C (to rates $\sim 27\%$ less than those at current- $p\text{CO}_2$). D_w rates were significantly lower at 28°C ($F_{3,8} = 46.18$, $p < 0.0001$; Fig. 1d), around $\sim 67\%$ below rates measured at current- $p\text{CO}_2$. This greater drop at 28°C compared to 26°C was a result of significant drops in light and dark production, versus drops just in dark production (Fig. 1e, f).

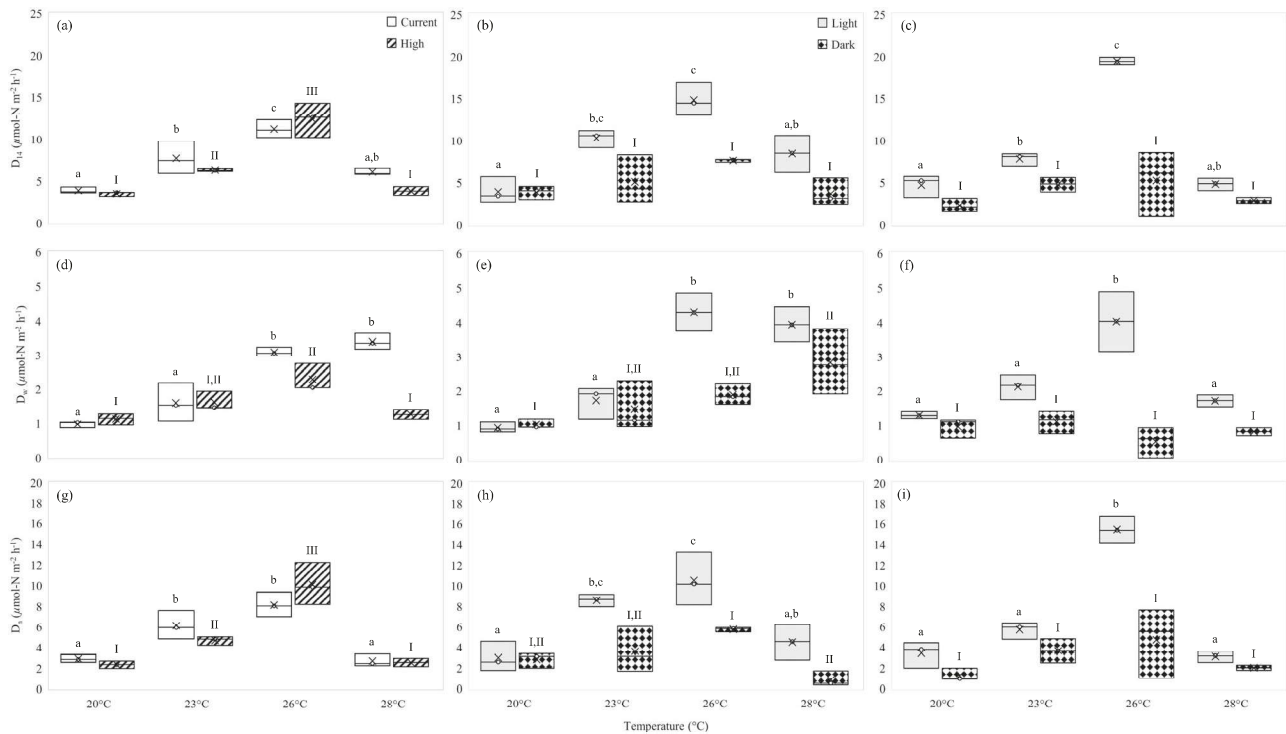


Fig. 1 | Effect of temperature on total denitrification (D_{14}), and denitrification of NO_3^- from the water column (D_w), and from nitrification (D_n) fluxes under current and high- $p\text{CO}_2$. Net diel (a) D_{14} , (d) D_w , and (g) D_n fluxes ($\mu\text{mol-N m}^{-2} \text{h}^{-1}$), under current- $p\text{CO}_2$ (open boxes) and high- $p\text{CO}_2$ (hatched boxes) conditions at three temperature offsets from control, 23°C . Letters identify significantly different means across temperatures under current- $p\text{CO}_2$ and numerals identify significantly different means across temperatures under high- $p\text{CO}_2$ conditions, where letters or numerals that are the same indicate no significant difference, as determined by a one-way ANOVA and post hoc Tukey's test. Light and dark fluxes for b/c D_{14} , e/f D_w , and h/i D_n fluxes

($\mu\text{mol-N m}^{-2} \text{h}^{-1}$) under current/high- $p\text{CO}_2$ conditions, respectively. Here, letters identify significantly different means across temperatures in light and numerals identify significantly different means across temperatures in dark cycles, where letters or numerals that are the same indicate no significant difference, as determined by a one-way ANOVA and post hoc Tukey's test. Statistical details are in Supplementary Tables 4 and 5. All boxes show mean values 'x', with the middle horizontal line indicating the exclusive median and the top and bottom edges indicating the start of the upper and lower quartiles, respectively.

The T_{opt} and Q_{10} denitrification rates changed with OA, with responses between dark and diel cycles varying between the total (D_{14}) and its components (D_w and D_n). In general, the Q_{10} of diel rates was greater than for dark rates, and D_w Q_{10} responded differently to OA than D_n and D_{14} . OA increased dark D_{14} and D_n Q_{10} from 3.14 and 3.28 under current- pCO_2 to 5.92 and 13.37, respectively, without affecting the T_{opt} of 26 °C (Table 1). In contrast, dark D_w Q_{10} decreased with OA, from a current- pCO_2 Q_{10} similar to that of D_{14} and D_n (3.33 to 1.61), also reducing the apparent T_{opt} by 5 °C, from 28 to 23 °C. These same Q_{10} and T_{opt} trends with D_{14} , D_n , and D_w were calculated from diel rates, with OA increasing diel D_{14} and D_n Q_{10} from 5.91 and 5.61 to 9.06 and 12.71, respectively, with T_{opt} at the same 26 °C, and D_w decreasing with OA from 5.20 to 3.19, with T_{opt} decreasing from 28 °C to 26 °C. Including light in diel N_2 production increased Q_{10} of D_w under both current and high- pCO_2 by 88% and 98%, respectively, D_{14} by 88% and 53%, respectively, and D_n under current- pCO_2 only, by 71%, with a slight decrease of 5% under high- pCO_2 .

N₂O fluxes

There was a significant interactive effect of warming and OA on sediment net diel N_2O responses ($F_{1,12} = 24.02$, $p = 0.0003$; Fig. 2a). Significant effluxes due to warming (162 ± 34 nmol-N $m^{-2} h^{-1}$; one-way: $F_{1,6} = 31.19$, $p = 0.0014$; Fig. 2a) diminished under combined warming and OA conditions (by ~64% to 59 ± 8 nmol-N $m^{-2} h^{-1}$), approaching OA-only efflux rates (63 ± 37 nmol-N $m^{-2} h^{-1}$). Similar interactive effects of OA and warming were measured under light conditions ($F_{1,12} = 18.72$, $p = 0.001$; Fig. 2b), where control sediments shifted from an influx of N_2O (99 ± 92 nmol-N $m^{-2} h^{-1}$) to an efflux under warming and/or OA treatment conditions. Warming resulted in the largest effluxes (190 ± 34 nmol-N $m^{-2} h^{-1}$) ($F_{1,12} = 17.73$, $p = 0.001$; Fig. 2b). In contrast, dark N_2O fluxes did not significantly vary with treatment ($p < 0.05$; Fig. 2c). N_2O contribution to gaseous N loss is <2% with its contribution increasing in warmer temperature but decreasing when warming and OA were considered

together (Table 2). Note, negative net N_2O contributions to gaseous N loss were calculated under control conditions (Table 2) because of the net N_2O uptake in the light (Fig. 2b) coupled with a net loss of N_2 (Fig. 1a).

Discussion

The influence of temperature on denitrification has been measured in dark anaerobic slurry incubations^{11–13} and in modelling studies¹⁷. However, by destroying the sediment vertical structure and removing the benthic-pelagic coupling and metabolic redox structure near the anoxic interface, anaerobic slurries omit the potential for substrate limitation to be captured in total denitrification rates. Reflecting this removal of substrate limitation in slurried sediments, Riekenberg et al. measured 3–36× higher N-uptake rates in slurries than measured in intact sediments. The whole core incubations used in the potential study simulate actual benthic-pelagic coupling, capturing the potential limitations of coupled nitrification-denitrification and diffusive NO_3^- supply from the water column for denitrifiers in the sediment. As such, the whole core N_2 flux measurements in the current study allowed us to understand temperature effects on denitrification based on NO_3^- from the water column (D_w) or from coupled nitrification/denitrification in the sediment (D_n).

Warming-related increases in N_2 and N_2O production under current- pCO_2

The temperature dependence of net D_w rates under current- pCO_2 was strong, with significant increases associated with warming. Similar to N_2 , N_2O fluxes increased with increasing temperature (Fig. 2c), which is consistent with an increase in denitrification rates leading to greater N_2O production¹¹. It is important to note that in this experiment we did not trace nitrate reduction to N_2O , but instead measured the net change in N_2O in the overlying water columns. As such, this net N_2O production may be a result of both denitrification and nitrification¹⁸. At projected warming (26 °C), net D_{14} and N_2O rate increases in the light (Fig. 1b, e, h). The increased production of both N_2 and N_2O in the light is likely indicative of coupled nitrification-denitrification¹⁹ as seen in other net heterotrophic sediments^{20,21}.

Under strong warming (28 °C), the decrease in D_{14} and D_n suggests a decrease in coupled nitrification-denitrification, despite a continued increase in D_w and N_2O formation (Figs. 1 and 2, respectively). However, other studies have observed an increase in nitrification activity and gene abundance with increasing temperatures¹⁶, suggesting that there is a decoupling of denitrification and nitrification instead of a decrease in nitrification rates. This decoupling might have resulted from an increase in competition for NO_3^- produced in the sediments through nitrification. Dissimilatory nitrate reduction to ammonium (DNRA) can outcompete

Table 1 | Dark and Diel Q_{10} and (T_{opt}) values for D_{14} , D_w , and D_n under current and high- pCO_2

	Dark			Diel		
	D_{14}	D_w	D_n	D_{14}	D_w	D_n
Current	3.14	3.33	3.28	5.91	5.20	5.61
	(26 °C)	(28 °C)	(26 °C)	(26 °C)	(28 °C)	(26 °C)
High	5.92	1.61	13.37	9.06	3.19	12.71
	(26 °C)	(23 °C)	(26 °C)	(26 °C)	(26 °C)	(26 °C)

Fig. 2 | N_2O fluxes across treatments. a Net diel, b light and c dark cycle rates (nmol $m^{-2} h^{-1}$) under current- pCO_2 at control and warming ($T \uparrow = \Delta + 3$ °C) temperatures and under high- pCO_2 conditions alone (CO_2) and with warming ($T \uparrow CO_2$). All boxes show mean values ‘x’, with the middle horizontal line indicating the exclusive median and the top and bottom edges indicating the start of the upper and lower quartiles, respectively. Letters identify significantly different means between temperatures under current- pCO_2 and numerals identify significantly different means across temperatures under high- pCO_2 conditions, where letters or numbers that are the same indicate no significant difference, as determined by a one-way ANOVA and post hoc Tukey’s test. Statistical details are in Supplementary Tables 4 and 5.

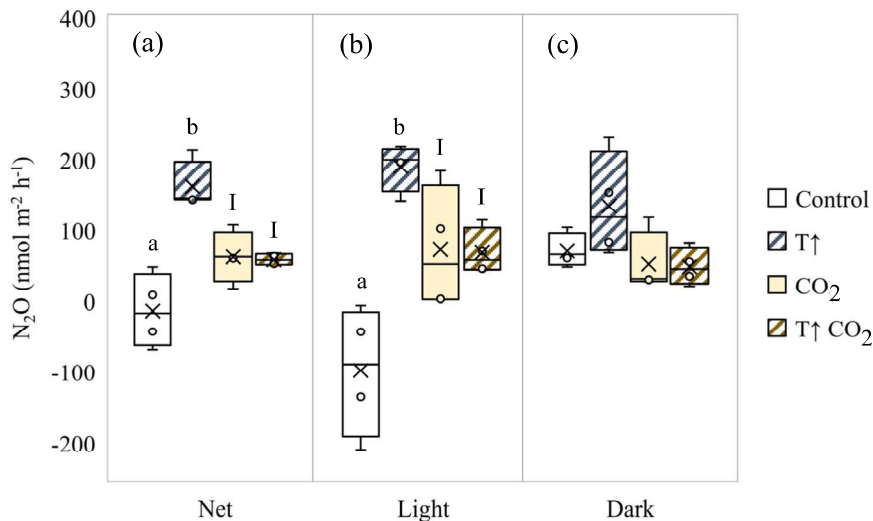


Table 2 | Light, dark, and net contribution (%) of N₂O to gaseous N loss

Current	Light	Dark	Net
23 °C	−0.96	1.4	−0.18
26 °C	1.28	1.76	1.45
High			
23 °C	0.93	1.1	1
26 °C	0.35	0.93	0.48

Table 3 | Mean (±SD) temperature (°C) and pCO₂ (µatm) conditions for each incubation

	Denitrification				N ₂ O			
	(1) Current		(2) High		(3) Current		(3) High	
	T (°C)	pCO ₂ (µatm)	T (°C)	pCO ₂ (µatm)	T (°C)	pCO ₂ (µatm)	T (°C)	pCO ₂ (µatm)
20 °C	21.0 (±0.1)	421.2 (±22.8)	20.9 (±0.4)	989.8 (±40.7)				
23 °C	23.2 (±0.1)	436.2 (±25.6)	23.2 (±0.1)	872.5 (±182.7)	22.96 (±0.39)	444.74 (±1.66)	22.96 (±0.62)	1001.71 (±28.35)
26 °C	25.6 (±0.5)	437.1 (±13.3)	25.8 (±0.2)	1011.1 (±248.6)	26.16 (±0.15)	500.83 (±7.22)	26.22 (±0.18)	1089.10 (±18.00)
28 °C	27.3 (±0.1)	411.8 (±52.9)	27.9 (±0.1)	989.5 (±40.7)				

Denitrification rate incubations at (1) current-pCO₂ (Sal = 24.4) and (2) high-pCO₂ (Sal = 17.7). Overlapping control present in the high-pCO₂ week had T = 23.1 ± 0.1 °C and pCO₂ = 458.7 ± 50.6 µatm. (3) N₂O flux incubation (Sal = 32).

denitrification for NO₃⁻ in increasingly reduced sediments under sustained anaerobic conditions^{22–24} and may be favourable under warming conditions¹⁷, which in turn would decouple nitrification-denitrification. The DIC to NH₄⁺ efflux ratio measured from the sediments (with a C:N of 16:1) in a parallel study under strong warming alone was 3.8²⁵ suggesting increased production of NH₄⁺ (Supplementary Table 2). DNRA is consistent with excess production of NH₄⁺ effluxed per mole of DIC compared to what is expected from the complete mineralisation of organic matter with a Redfield C:N ratio of 106:16²⁶ or the in situ sediment organic matter, which had a C:N ratio of 16:1²⁵.

Reduced denitrification and N₂O production under warming and ocean acidification

A decrease in dark and diel *D_w* rates and N₂O fluxes at warmer temperatures (>23 °C) elevated-pCO₂ (Figs. 1f, e and 2), may indicate unfavourable conditions for denitrifiers. A mesocosm study of temperate, Scottish estuarine sediments found that 16 S rRNA (*nirS* and *amoA*) gene abundances responsible for nitrogen cycling were lower in combined stressor treatments than at elevated temperatures under current-pCO₂¹⁶, indicating a reduction in the respective activities of denitrifiers and nitrifiers. However, the short duration of the incubations here would better reflect suppression of activity when exposed to unfavourable conditions, which may lead to a reduction of denitrifiers/nitrifiers in the long term.

Under strong warming (28 °C) and high-pCO₂ there was a greater decrease in *D₁₄* than measured under current-pCO₂, despite an equal decrease in *D_n* (Fig. 1a, g). This gap reflects the large decrease in *D_w* at increased temperatures under high-pCO₂ conditions only (Fig. 1d). The decrease in *D_w* and nitrification rates (included in *D₁₄* and *D_n*) that resulted from OA with strong warming may also reflect changes in gene abundance¹⁶. Unlike sediment responses to strong warming under current-pCO₂, sediment responses under high-pCO₂ did not suggest an increased

role of DNRA in NO₃⁻ reduction²⁵. This difference may be a result of reduced nitrification¹⁶ potentially limiting the coupling with DNRA. For example, pushing sediments to DNRA might not only reduce N₂O production, but it might increase N₂O consumption as organisms carrying out DNRA have been found to have atypical *NosZ* genes²⁷. Alternatively, OA may have a similar inhibitory effect on DNRA as has been observed for denitrification and nitrification¹⁶.

Q₁₀ values for denitrification affected by ocean acidification

Under current-pCO₂, dark denitrification rates appeared to be strongly dependent on temperature changes (Table 3). Q₁₀ values for denitrification previously reported for subtropical unvegetated coastal sediments^{11,13} are similar to the values in the current study. Dark denitrification Q₁₀ values calculated here under current-pCO₂ (3.14–3.33; Table 3) are closer to those reported by Canion et al.¹³ (3.8–5.0) than by Tan et al.¹¹ (1.9–2.7). Instead, Tan et al.¹¹ denitrification Q₁₀ values appear to reflect Q₁₀ values of temperate and polar regions^{13,28,29}. Both Tan et al.¹¹ and Canion et al.¹³ Q₁₀ ranges were calculated from potential denitrification rates, compared to the actual denitrification rates measured here. Regardless, this strong positive Q₁₀ is consistent with N₂O production increasing with warming, as was also measured in this study (Fig. 2), supporting previous findings that increases in temperature and denitrification activity will increase the occurrence of denitrification and the production of N₂O¹¹.

The *T_{opt}* of *D_w* rates in this study was 28 °C, the experimental maximum temperature (the actual *T_{opt}* may have been higher). This is comparable to previously reported potential optimum temperatures of at least 30 °C^{11–13}. However, *D₁₄* and *D_n* rates in the current study had a *T_{opt}* of 26 °C (Table 3). The inclusion of nitrification in these measurements suggests that nitrification may have a lower *T_{opt}* than denitrification³⁰. Although, sediment nitrification rates at a similar latitude in the North Ariake Sea in Japan, had an estimated *T_{opt}* of 28 °C³¹, the reason for the rate decrease after only 26 °C remains speculative.

In the current study, for the first time, the effect of OA on the temperature sensitivity of denitrification rates has been calculated. In the dark, OA reduced temperature stimulation of *D_w* rates (Fig. 1e, f), reducing Q₁₀ from 3.33 to 1.61. N₂O flux rates reflected this reduced temperature sensitivity in denitrification rates, with lower dark and net N₂O effluxes under combined warming and OA conditions (Fig. 2b, c).

N₂O fluxes identify potential limitations in sediment denitrification

Sediments under ambient conditions in the current study had the highest denitrification rates in the light period yet were a sink of N₂O, and had reduced denitrification rates in the dark, despite becoming a source of N₂O. Sediment uptake of N₂O is not uncommon^{32–34} and relates to its use by denitrifiers as a terminal electron acceptor for OM degradation in the absence of NO_x³⁴, or its use in the oxidation of reduced sulfur compounds to produce N₂³⁵. NO_x availability in the oligotrophic Clarence Estuary waters was low (<2 µM), forcing denitrifiers to compete for NO_x with the photoautotrophic microorganisms and bacteria living within the photic surface sediments. As a result, denitrifiers were likely forced to use N₂O despite the preference for NO_x as an electron acceptor^{36,37}. This competition with photoautotrophs is absent in the dark, allowing for the uninhibited utilisation of NO_x by denitrifiers. As such, the preference of NO_x as an electron acceptor coupled with the excess of NO_x availability would promote the incomplete reduction of NO_x to N₂O, and not N₂^{36,37}. Alternatively, nitrification may have been responsible for driving N₂O fluxes and this may have been alleviated under light conditions when oxygen concentrations were higher³⁸.

N₂O production rates can be accelerated when concentrations of NH₄⁺ and NO_x are elevated⁶, or when organic matter is limited³⁹ and/or refractory⁴⁰. N₂O flux was greatest in both the light and dark under warming conditions relative to control or OA-amended treatments (Fig. 2). Elevated temperatures are expected to increase NH₄⁺ and NO_x availability²⁵ due to

thermal stimulation of organic matter remineralisation^{41,42} and nitrification³¹. This, coupled with the increased denitrification measured in this study (Fig. 1), accounts for the significant increase in net N₂O effluxes under conditions of warming alone.

Under acidified conditions, warming did not affect sediment net and light/dark N₂O flux (Fig. 2) despite the interactive effect that was found for *D_w* (Fig. 1d). This effect of OA on N₂O flux was two-fold. OA reduced denitrification rates at elevated temperatures, reducing the potential for light and dark production of N₂O. However, in the light, sediments were still a source of N₂O relative to control conditions. Previous findings show that OA increases the availability of NO_x to the sediments²⁵ with a likely stimulation of nitrification from increased O₂ production by photoautotrophs¹⁹, possibly reducing the need for denitrifiers to utilise N₂O in their reduction of OM. Alternatively, a reduced microbial electron transfer efficiency during denitrification under OA conditions may have encouraged N₂O production, versus its reduction⁴³.

Previous studies of the effect of temperature on denitrification have been limited to potential rates measured in the dark^{11,13}. This study has shown that light and OA alter the diel *Q₁₀*, *T_{opt}*, and overall response of denitrification activity. This is chiefly due to the potential for OA to stimulate photoautotrophic activity in the light⁴⁴. Because photoautotrophic production could either slow the rates of denitrification due to increased competition for nitrate or increased dissolved oxygen in the experiment^{45,46}, or stimulate denitrification with a coupled increase in nitrification rates^{19,21}, the resulting effects are polarised. Further complications emerge when you consider the possibility that OA may make conditions unfavourable for denitrifiers¹⁶. However, in the present study, denitrification was generally greater in the light than in the dark (Fig. 1), suggesting that nitrification likely increased substrate availability and alleviated competition between denitrifiers and photoautotrophs. In contrast, OA has the potential to reduce the stimulating effect of warming on *D_w* (Fig. 1d) and N₂O production (Fig. 2a) by up to 64%. These contrasting stimulating and reducing effects on denitrification and N₂O highlight the need to (1) include a full diel cycle to determine the temperature sensitivity of sediment processes, and (2) consider the interactions of future climate conditions. Failure to do so may hinder our ability to make accurate future projections of climate-related impacts. This study was only undertaken at one site. Further, work should be undertaken at sites with different environmental conditions to see if the responses of denitrification and N₂O sediment-water fluxes to warming and OA are similar. Moreover, our warming treatments were offset from the ten-year average for the Clarence estuary. Additional studies should be undertaken in winter and summer with warming treatments offset from average seasonal temperatures to see if the responses of denitrification and N₂O sediment-water fluxes to warming and OA are similar under different seasonal conditions and strive to include longer-term (months) experiments to reflect the chronic processes of warming and OA.

Methods

Site description

Cores were collected on three separate sampling excursions within the same 4 m × 12 m in the Clarence River, Yamba, NSW, Australia (29°24.21'S, 153°19.44'E; Supplementary Fig. 1). Two excursions used subtidal sediments (Summer—January 2018) with ~0.3–1.0 m of overlying water at low-tide, to measure denitrification rates. The third excursion used intertidal sediments that were collected as part of a separate study (Spring—September 2019). Intertidal sediments at this site are only exposed for up to 3 h during very low tides and are subtidal the remainder of the time. The average sea level at high tide is approximately 2 m above the sediment surface. Subtidal sediments (0–2 cm) had a higher porosity (0.43) and organic matter (OM) content (~3.5% of dry weight), determined from mass loss after combustion (490 °C for 4 h) of dried sediment (60 °C), relative to intertidal sediments (0–2 cm), which had a porosity of ~0.23 and OM content of ~1.34%. The top 10 cm of sediments were characterised via dry sieving analysis^{47,48}, with both subtidal and intertidal sediments having a well-sorted sandy-mud grain size distribution (Supplementary Table 3). Dissolved inorganic nitrogen (DIN) concentrations at the time of this study (~1.19–2.40 μM, Table 4) were relatively low and consistent with previous studies in the Clarence River (<2 μM¹⁶), as a result of low nutrient loading in the catchment area⁴⁹. Temperature (±0.3 °C) and salinity (±1%) were measured over 24 h using a submerged Hydrolab (HL7) at the site. The mean daily water temperature at the site ranged from 21.3 ± 1 °C (max 24 °C) in September to 23.5 ± 1 °C (max 26 °C) in January. Salinity varied from 10–35 over the tidal cycle at both times of year.

Core collection

Acrylic cores (9 cm diameter × 47 cm) were used to collect sediments (around 20 cm depth allowing for ~1.8 L of overlying site water). To measure denitrification rates, 33 sediment cores were collected on January 09th, 2018 and 27 cores were collected on January 16th, 2018. Cores were collected from inundated sediment at low tide to ensure all sediments were subtidal. To measure N₂O fluxes, 16 cores were collected on September 16th, 2019. Large burrow openings were avoided during all collections to reduce the variability among cores that would otherwise result from the occasional inclusion of large macrofauna⁵⁰. In addition to sediment cores, 700 L of site water was collected on each excursion to fill a laboratory incubation set-up, in which all cores were submerged within 6 h of collection.

Climate scenarios

This investigation considered the temperature dependence of denitrification rates under both current and high-*p*CO₂ conditions (~480 and ~1000 μatm, respectively). As such, sediments were subjected to both cooling and warming, covering an 8 °C range from 20 to 28 °C. Control temperatures were defined as the ten-year average annual sea surface temperature in Yamba, ~23 °C (17–27 °C)⁵¹. Three discrete temperature offsets from “control” were selected, (1) the projected end-of-century SST, Δ+3 °C (RCP8.5⁹), (2) a greater warming condition, Δ+5 °C, and (3) a lower temperature condition, Δ–3 °C. Although sediments occasionally experience these offset temperatures throughout the year, the objective of this study was not to stress the sediments, but instead to quantify the effect that incremental temperature increases have on benthic denitrification rates. Moreover, the generation time of the dominant microbial members of unvegetated estuarine sediments was from 6–15 h^{52,53}, thus sediments were given sufficient time for multiple generations during a 48–72 h acclimation period to treatment conditions. Temperatures were maintained at 23 ± 0.5 °C (control), 26 ± 0.5 °C (RCP8.5 projected warming), 28 ± 0.5 °C (stronger warming), and 20 °C (cooling) throughout the experiment. OA conditions were simply defined as a doubling of current mean *p*CO₂ (417 μatm⁵⁴), under the high emission scenario (RCP8.5⁸). To complement the denitrification incubation, N₂O incubations used two temperatures, current mean ambient temperature (23 °C) and projected warming (26 °C), in a full factorial design with current and high-*p*CO₂ levels (~450 and 900 μatm, respectively), to focus on projected warming and OA effects.

Table 4 | Mean (±SD) DIN concentration (μM) at the start of dark (Start D), transition to light (D/L) and end of light (End L) incubations

	Current- <i>p</i> CO ₂			High- <i>p</i> CO ₂		
	Start (D)	D/L	End (L)	Start (D)	D/L	End (L)
20 °C	1.19	2.01	2.02	1.85	4.22	6.66
	(±0.01)	(±1.14)	(±0.45)	(±0.27)	(±0.74)	(±1.36)
23 °C	1.85	5.58	4.00	2.42	4.81	6.11
	(±0.16)	(±1.15)	(±0.27)	(±1.01)	(±0.90)	(±1.39)
26 °C	1.88	6.25	4.47	1.97	5.39	9.61
	(±0.42)	(±0.38)	(±2.10)	(±0.31)	(±0.14)	(±1.36)
28 °C	2.37	14.47	15.52	2.40	6.86	14.68
	(±0.18)	(±2.66)	(±1.81)	(±0.58)	(±0.79)	(±4.42)

Incubation setup

In the laboratory, depending on the incubation, 4 to 5 tanks were fitted with a thermo-regulating aquarium pump to maintain temperature (± 0.1 °C). Current- $p\text{CO}_2$ tanks were aerated with ambient laboratory air (~ 450 μatm) via an air pump and airstones, whereas high- $p\text{CO}_2$ tanks were aerated with an enriched- CO_2 airstream (~ 1000 μatm) to simulate the desired future atmospheric CO_2 conditions (~ 900 μatm ; Table 3) and to ensure water columns were saturated with O_2 prior to the start of incubations (O_2 concentrations were ~ 230 $\mu\text{mol L}^{-1}$ at the start of incubations and remained above 152 $\mu\text{mol L}^{-1}$ for all treatments, see⁴⁴ for further detail). DIN concentrations were low at the start of incubations with details of start and end concentrations in Table 4). DIC concentrations were determined using an AIRICA system (MARIANDA, Kiel) via infrared absorption using a LICOR LI-7000, and corrected for accuracy against certified reference material, batch #171⁵⁵ for both the denitrification and N_2O incubations. DIC was coupled with total alkalinity measurements using potentiometric titration on a Metrohm 869 Compact Sample Changer and an 848 Titrino plus dosing unit, according to the open-cell method described in Dickson⁵⁶ for N_2O incubations, and pH measurements made with a Hach HQ40d Multiprobe metre and probe calibrated to 3-point standard buffer scale (National Institute for Standards and Technology—NIST, $R^2 = 0.99$) for denitrification incubations to calculate $p\text{CO}_2$ offsets using CO_2SYS following methods described in Simone et al.^{44,57}

Water columns within cores were stirred throughout the incubations via the interaction of magnetic stir bars with an external rotating magnet (60 rpm). Stir bars were positioned ~ 5 cm above the sediment surface to ensure sediments were not disturbed^{58,59}. High-pressure sodium lamps (400 W; PHILIPS Son-T Argo 400) were positioned above the tanks so that each core would receive ~ 270 – 280 $\mu\text{mol quanta m}^{-2} \text{s}^{-1}$ of photosynthetically active radiation (PAR) at the water surface, equivalent to mean daytime field conditions measured at 1 m depth with a HOBO light logger. These lamps were turned on in the mornings to simulate the day in line with natural diel light cycling and followed a $\sim 12:12$ h light:dark cycle, similar to that in situ.

For the denitrification incubations four temperature treatment tanks (20 °C, 23 °C (control), 26 °C, and 28 °C) were each filled with ~ 80 L of site water. Due to limited space, two separate denitrification incubations were done using the same laboratory setup to investigate N_2 production responses to temperatures under current (~ 450 μatm ; week of January 16th, 2018) and high- $p\text{CO}_2$ conditions (~ 900 μatm ; week of January 09th, 2018). Sediment cores were randomly allocated to the tanks. Two sets of 3 cores ($n = 6$) were placed uncapped in each tank, except for the control tank, which had an additional 3 cores submerged ($n = 9$). The additional 3 cores in the control tank were used for analysis of background isotope ratios in sediment and water compartments. For the high- $p\text{CO}_2$ incubation, an additional tank was included to provide an overlapping control (control temperature, current- $p\text{CO}_2$) and allow for comparison among treatments across the two incubations. The overlapping control cores were used to verify that sediments in the two separate incubations were behaving the same way in the absence of any treatment and to control for any differences between incubations resulting from the collection of sediments and overlying water at different times.

For the N_2O incubations, four tanks were used to provide a fully factorial design of two temperatures (23 °C and 26 °C) at both current and high- $p\text{CO}_2$ (~ 460 μatm and ~ 900 μatm), with each tank receiving four cores.

Sampling design and analysis

Denitrification. Cores were left open to acclimate in tank water with warming and OA conditions imposed for 48–72 h, before being capped to begin diel incubations, which encompassed an entire dark/light cycle. At the beginning of both the light and dark cycles, the starting concentration of NO_3^- was determined for each core; 20 mL of water was syringe sampled from a resealable port in the lid of each core, filtered (0.45 μm cellulose acetate) into duplicate 12 mL polyethylene vials (2 mL

headspace), and stored frozen until analysis using a LachatTM flow-injection system⁶⁰. Three cores per treatment were then labelled at the beginning of the dark period with a 15 mmol- $^{15}\text{N L}^{-1}$ (99% $^{15}\text{N-KNO}_3$) stock solution to reach a final DIN concentration in cores of ~ 16.9 $\mu\text{mol L}^{-1}$, enriching 95% of the NO_3^- pool and 89% of the DIN pool with the added ^{15}N , to determine the changes to microbial reduction pathways through isotope pairing of N_2 . The three remaining cores in each treatment were labelled to the same enrichment at the beginning of the light period. Label additions were done separately at the beginning of dark and then at the beginning of light to isolate the isotope accumulation and transfers for each part of the diel cycle.

After ~ 10 h in the dark or light, labelled cores were sacrificed. Nitrogen stable isotope ratios ($\delta^{15}\text{N}$) of N_2 were determined from sample water collected from sealed cores via syringe, without bubbles, in 12 mL glass exetainers preserved with 20 μL of saturated HgCl_2 and stored with no headspace at room temperature. The additional three cores in the control tank without label addition were sacrificed in the same way and used as background isotope references. Sediments from background cores were used to determine the carbon and nitrogen content (% $\delta^{13}\text{C}$ and $\delta^{15}\text{N}$) of organic matter. Homogenised surface sediments were dried (60 °C) and acidified (carbon) or rinsed with KCl (2 M, nitrogen) to remove inorganic content settled or adsorbed on the sediment. Dry samples were then analysed on a Thermo Finnigan Flash EA 112 coupled via a Thermo Conflo III to a Thermo Delta V Plus IRMS to verify that the C:N of surface sediments (0–5 cm) and $\delta^{13}\text{C}$ and $\delta^{15}\text{N}$ values were comparable across the two incubations. A 2 mL He headspace was later added to the N_2 samples ~ 24 h prior to analysis. N_2 concentrations and isotope ratios were determined from the He headspace via isotope ratio mass spectrometry (IRMS), using a Thermo Trace Ultra gas chromatograph (GC) equipped with an autosampler⁶¹ coupled to a Delta V Plus IRMS via a Thermo Conflo III interface. All values are reported with respect to N_2 in the air. Immediately before and after samples were run, N_2 standards with known % $^{29}\text{N}_2$ and $^{30}\text{N}_2$ were used to correct for interference in the ion source caused by the generation of NO. The isotope pairing technique (IPT) of Nielsen (1992) was used to calculate actual N_2 loss (D_{14}) from the production of $^{29}\text{N}_2$ and $^{30}\text{N}_2$. This method also assumes no anammox is present, which was confirmed by a separate incubation (Supplementary Method 1), in which anammox was absent from all sediment depths (0 to 90 mm) (Supplementary Fig. 2). The absence of anammox meant that the original IPT⁶² could be used to calculate denitrification in the intact core incubations.

Denitrification (D_{14}) was then separated into two components, denitrification from (1) NO_3^- diffusing into the sediments from the water column (D_w) and (2) NO_3^- produced within the sediments via nitrification (D_n)⁶², using the frequency of ^{14}N and ^{15}N substrate available. All final rates were presented as $\mu\text{mol-N m}^{-2} \text{d}^{-1}$, assuming a 12:12 h light:dark cycle.

N_2O fluxes. Cores were left open to acclimate in tank water under temperature and OA-amended conditions (with no substrate amendment) for ~ 48 h before being capped to begin incubations. Cores were capped prior to the simulation of daylight, with water samples collected immediately before lights were switched on, by gently syringe-sampling water (20 mL) from resealable ports fitted in each core lid. Water samples (6 mL) were then injected into duplicate 12 mL He flushed and sealed exetainers preserved with 20 μL HgCl_2 without letting air escape, overturned, and allowed to equilibrate under pressure at room temperature (21 °C) for >48 h. Cores were left in the light for ~ 3 h before end-of-cycle sampling using the same method outlined for the start of the incubation. Cores were then uncapped and water columns were allowed to recirculate. In line with natural light cycling, the lights were turned off, and cores were resealed for dark sampling. Water collection for N_2O samples in the dark was identical to that in the light. The time between the start and end of N_2O incubations was ~ 3 h.

Dissolved N_2O concentrations were determined from the equilibrated gas in the pressurised exetainers, using gas chromatography (GC, Shimadzu GC-9A) equipped with an electron capture detector⁶³. A five-point

standard curve was used to calibrate the GC with a precision typically >99%. The headspace concentrations (y in Eq. 1, ppm) were used to calculate the dissolved concentration (mol L^{-1}) at equilibration temperature (21 °C) and subsequently adjusted to calculate the dissolved concentrations for the respective treatment temperatures (nmol L^{-1}).

$$N_2O = \frac{((y - Bg) \times 10^{-6}) \times ((P \times \beta_{RT} \times V_w) + (V_h))}{V_w \times 10^9 \times P / (R \times T)} \quad (1)$$

where β_{RT} is the dimensionless Bunsen solubility coefficient ($\text{mL gas mL H}_2\text{O}^{-1} \text{atm}^{-1}$) calculated at room temperature for N_2O^{64} , P is the atmospheric pressure of the headspace in the exetainer, V_w and V_h is the volume of liquid sample and headspace volumes, respectively. R is the constant for an ideal gas ($0.082057 \text{ L atm K}^{-1} \text{ mol}^{-1}$), T is the treatment temperature (°K), and Bg is the background N_2O concentration (mol L^{-1}) measured in He flushed 'blank' exetainers.

Data analyses

Temperature sensitivity coefficients (Q_{10} values) were used to evaluate the response of dark and diel rates of D_w , D_n , and D_{14} to temperature increases of 10 °C. This was expressed simply as an exponential function:

$$Q_{10} = \left(\frac{R_2}{R_1} \right)^{10 \text{ } ^\circ\text{C} / (T_{\text{opt}} - T_1)} \quad (2)$$

where R_1 and R_2 are the denitrification rates (D_w , D_n , or D_{14}) measured at temperatures 20 °C (T_1) and optimal temperatures (T_{opt}), respectively. T_{opt} was defined as the incubation temperature for which denitrification rates were highest.

Statistical analyses

Statistical tests were conducted on denitrification and N_2O flux rates using MATLAB⁶⁵. Statistical significance was generally defined as $\alpha < 0.05$. All datasets were checked for homogeneity of variances (Levene's test) before further analysis. If Levene's test returned a significant result, data was log-transformed. If data could not be log-transformed, an α of 0.01 was used to limit type I errors.

Net variability with temperature and CO_2 . Net fluxes among treatments were compared to identify the effect of temperature and $p\text{CO}_2$ condition. A one-way analysis of variance (ANOVA) was used to investigate the effect of high- $p\text{CO}_2$ at each temperature. A two-way ANOVA then examined differences among temperatures ($n = 4$ or 2, for denitrification and N_2O , respectively) at each level of $p\text{CO}_2$ ($n = 2$) and identified any interacting effects. Finally, a separate one-way ANOVA was run for each level of $p\text{CO}_2$ to investigate sediment responses across temperatures and to further investigate significant interactions identified in the two-way ANOVA. Post hoc Tukey's tests were used to determine which scenarios had similar or different responses.

Diel variability of denitrification rates with temperature. To further investigate changes observed in net fluxes, differences between dark and light cycles were compared. First, a two-way analysis of variance (ANOVA) was used to examine differences among temperatures ($n = 4$), light conditions ($n = 2$), and whether light conditions significantly affected temperature response for cores in the current and high- $p\text{CO}_2$ climates separately. Following this, a one-way ANOVA was run for each light condition to investigate any significant interaction found in the two-way ANOVA and to consider the individual temperature responses. If a significant effect was found in the one-way ANOVAs, post hoc Tukey's tests were used to determine which treatments were significantly different from one another.

Treatment effects on light and dark N_2O fluxes. Two-way ANOVAs were used to investigate potential differences in sediment N_2O flux

responses to warming ($n = 2$) and $p\text{CO}_2$ ($n = 2$) in the light and dark, where separate one-way ANOVAs were run for each level of $p\text{CO}_2$ to further investigate significant interactions identified in the two-way ANOVA.

Reporting summary

Further information on research design is available in the Nature Portfolio Reporting Summary linked to this article.

Data availability

The following datasets are publicly available: Dataset S1. N_2 data (Simone et al., -ds01)^{25,44,57}, Dataset S2. N_2O data (Simone et al., -ds02)^{25,44,57}, Dataset S3. Anaerobic ammonium oxidation slurry data (Simone et al., -ds03)^{25,44,57}. <https://doi.org/10.5281/zenodo.10525246>.

Received: 10 April 2023; Accepted: 26 March 2024;

Published online: 10 April 2024

References

1. Rockström, J. et al. A safe operating space for humanity. *Nature* **461**, 472–475 (2009).
2. Gruber, N. & Galloway, J. N. An Earth-system perspective of the global nitrogen cycle. *Nature* **451**, 293–296 (2008).
3. Nixon, S. W. et al. The fate of nitrogen and phosphorus at the land-sea margin of the North Atlantic Ocean. *Biogeochemistry* **35**, 141–180 (1996).
4. Ward, B. B. How nitrogen is lost. *Science* (80-). **341**, 352–353 (2013).
5. Seitzinger, S. et al. Denitrification across landscapes and waterscapes: a synthesis. *Ecol. Appl.* **16**, 2064–2090 (2006).
6. Quick, A. M. et al. Nitrous oxide from streams and rivers: a review of primary biogeochemical pathways and environmental variables. *Earth-Sci. Rev.* **191**, 224–262 (2019).
7. Myhre, G. et al. Radiative forcing of the direct aerosol effect from AeroCom Phase II simulations. *Atmos. Chem. Phys.* **13**, 1853–1877 (2013).
8. IPCC. *Special Report on the Ocean and Cryosphere in a Changing Climate*. (IPCC, 2019).
9. Collins, M. et al. Long-term climate change: projections, commitments and irreversibility. In: *Climate Change 2013: The Physical Science Basis. Contribution of Working Group I to the Fifth Assessment Report of the Intergovernmental Panel on Climate Change* (eds. Stocker, T. F. et al.) 1029–1136 (Cambridge University Press, Cambridge, United Kingdom and New York, NY, USA, 2013).
10. Zeebe, R. E. & Wolfgladrow, D. CO_2 in seawater: equilibrium, kinetics, isotopes. In *Elsevier Oceanography Series, 65* (Elsevier, Amsterdam, London, New York, 2001).
11. Tan, E. et al. Warming stimulates sediment denitrification at the expense of anaerobic ammonium oxidation. *Nat. Clim. Chang.* **10**, 349–355 (2020).
12. Zhou, S., Borjigin, S., Riya, S., Terada, A. & Hosomi, M. The relationship between anammox and denitrification in the sediment of an inland river. *Sci. Total Environ.* **490**, 1029–1036 (2014).
13. Canion, A. et al. Temperature response of denitrification and anammox reveals the adaptation of microbial communities to in situ temperatures in permeable marine sediments that span 50 in latitude. *Biogeosciences* **11**, 309–320 (2014).
14. Brin, L. D., Giblin, A. E. & Rich, J. J. Similar temperature responses suggest future climate warming will not alter partitioning between denitrification and anammox in temperate marine sediments. *Glob. Chang. Biol.* **23**, 331–340 (2017).
15. Wan, R., Chen, Y., Zheng, X., Su, Y. & Li, M. Effect of CO_2 on microbial denitrification via inhibiting electron transport and consumption. *Environ. Sci. Technol.* **50**, 9915–9922 (2016).
16. Currie, A. R. et al. Marine microbial gene abundance and community composition in response to ocean acidification and elevated

- temperature in two contrasting coastal marine sediments. *Front. Microbiol.* **8**, 1599 (2017).
17. Kelly-Gerrey, B. A., Trimmer, M. & Hydes, D. J. A diagenetic model discriminating denitrification and dissimilatory nitrate reduction to ammonium in a temperate estuarine sediment. *Mar. Ecol. Prog. Ser.* **220**, 33–46 (2001).
 18. Freing, A., Wallace, D. W. R. & Bange, H. W. Global oceanic production of nitrous oxide. *Philos. Trans. R. Soc. B Biol. Sci.* **367**, 1245–1255 (2012).
 19. An, S. & Joye, S. B. Enhancement of coupled nitrification-denitrification by benthic photosynthesis in shallow estuarine sediments. *Limnol. Oceanogr.* **46**, 62–74 (2001).
 20. Risgaard-Petersen, N. Coupled nitrification-denitrification in autotrophic and heterotrophic estuarine sediments: on the influence of benthic microalgae. *Limnol. Oceanogr.* **48**, 93–105 (2003).
 21. Welsh, D. T. et al. Denitrification, nitrogen fixation, community primary productivity and inorganic-N and oxygen fluxes in an intertidal *Zostera noltii* meadow. *Mar. Ecol. Prog. Ser.* **208**, 65–77 (2000).
 22. Tiedje, J. M. Ecology of denitrification and dissimilatory nitrate reduction to ammonium. *Biol. Anaerob. Microorg.* **717**, 179–244 (1988).
 23. Brunet, R. C. & Garcia-Gil, L. J. Sulfide-induced dissimilatory nitrate reduction to ammonia in anaerobic freshwater sediments. *FEMS Microbiol. Ecol.* **21**, 131–138 (1996).
 24. Christensen, P. B., Rysgaard, S., Sloth, N. P., Dalsgaard, T. & Schwærter, S. Sediment mineralization, nutrient fluxes, denitrification and dissimilatory nitrate reduction to ammonium in an estuarine fjord with sea cage trout farms. *Aquat. Microb. Ecol.* **21**, 73–84 (2000).
 25. Simone, M. N., Oakes, J. M., Schulz, K. G. & Eyre, B. D. Ocean acidification modifies the impact of warming on sediment nitrogen recycling and assimilation by enhancing the benthic microbial loop. *Mar. Ecol. Prog. Ser.* **681**, 53–69 (2022).
 26. Redfield, A. C. *Development of a New England Salt Marsh*. Vol. 42, 201–237 (Ecological Society of America, 1972).
 27. Sanford, R. A. et al. Unexpected nondenitrifier nitrous oxide reductase gene diversity and abundance in soils. *Proc. Natl. Acad. Sci. USA.* **109**, 19709–19714 (2012).
 28. Ambus, P. Control of denitrification enzyme activity in a streamside soil. *FEMS Microbiol. Ecol.* **11**, 225–234 (1993).
 29. Palacin-Lizarbe, C., Camarero, L. & Catalan, J. Denitrification temperature dependence in remote, cold, and N-poor lake sediments. *Water Resour. Res.* **54**, 1161–1173 (2018).
 30. Rysgaard, S., Glud, R. N., Risgaard-Petersen, N. & Dalsgaard, T. Denitrification and anammox activity in Arctic marine sediments. *Limnol. Oceanogr.* **49**, 1493–1502 (2004).
 31. Isnansetyo, A., Getsu, S. A. I., Seguchi, M. & Koriyama, M. Independent effects of temperature, salinity, ammonium concentration and pH on nitrification rate of the Ariake seawater above mud sediment. *HAYATI J. Biosci.* **21**, 21–30 (2014).
 32. Jensen, H. B., Jørgensen, K. S. & Sørensen, J. Diurnal variation of nitrogen cycling in coastal, marine sediments. *Mar. Biol.* **83**, 177–183 (1984).
 33. Miller, L. G., Oremland, R. S. & Paulsen, S. Measurement of nitrous oxide reductase activity in aquatic sediments. *Appl. Environ. Microbiol.* **51**, 18–24 (1986).
 34. Kieskamp, W. M., Lohse, L., Epping, E. & Helder, W. Seasonal variation in denitrification rates and nitrous oxide fluxes in intertidal sediments of the western Wadden Sea. *Mar. Ecol. Prog. Ser. Oldend.* **72**, 145–151 (1991).
 35. Dalsgaard, T. & Bak, F. Effect of acetylene on nitrous oxide reduction and sulfide oxidation in batch and gradient cultures of *Thiobacillus denitrificans*. *Appl. Environ. Microbiol.* **58**, 1601–1608 (1992).
 36. Betlach, M. R. & Tiedje, J. M. Kinetic explanation for accumulation of nitrite, nitric oxide, and nitrous oxide during bacterial denitrification. *Appl. Environ. Microbiol.* **42**, 1074–1084 (1981).
 37. Schlegel, H. G. & Zaborosch, C. *General Microbiology*. (Cambridge University Press, 1993).
 38. Jørgensen, K. S., Jensen, H. B. & Sørensen, J. Nitrous oxide production from nitrification and denitrification in marine sediment at low oxygen concentrations. *Can. J. Microbiol.* **30**, 1073–1078 (1984).
 39. Appelo, C. A. J. & Postma, D. *Geochemistry, Groundwater and Pollution*. (CRC Press, 2005).
 40. Megonigal, J. P., Hines, M. E. & Visscher, P. T. Anaerobic metabolism: linkages to trace gases and aerobic processes. In *Treatise on Geochemistry* pp. 317–424 (Elsevier, 2004).
 41. Piontek, J. et al. Effects of rising temperature on the formation and microbial degradation of marine diatom aggregates. *Aquat. Microb. Ecol.* **54**, 305–318 (2009).
 42. Thamdrup, B. & Fleischer, S. Temperature dependence of oxygen respiration, nitrogen mineralization, and nitrification in Arctic sediments. *Aquat. Microb. Ecol.* **15**, 191–199 (1998).
 43. Su, X. et al. Stimulation of N₂O emission via bacterial denitrification driven by acidification in estuarine sediments. *Glob. Chang. Biol.* 1–16 <https://doi.org/10.1111/gcb.15863> (2021).
 44. Simone, M. N., Schulz, K. G., Oakes, J. M. & Eyre, B. D. Warming and ocean acidification may decrease estuarine dissolved organic carbon export to the ocean. *Biogeosciences* **18**, 1823–1838 (2021).
 45. Risgaard-Petersen, N., Rysgaard, S., Nielsen, L. P. & Revsbech, N. P. Diurnal variation of denitrification and nitrification in sediments colonized by benthic microphytes. *Limnol. Oceanogr.* **39**, 573–579 (1994).
 46. Rysgaard, S., Christensen, P. B. & Nielsen, L. P. Seasonal variation in nitrification and denitrification in estuarine sediment colonized by benthic microalgae and bioturbating infauna. *Mar. Ecol. Prog. Ser.* **126**, 111–121 (1995).
 47. Lewis, D. W. & McConchie, D. *Sample Treatment in the Laboratory*. In *Analytical Sedimentology*. (Springer, Boston, MA, 1994).
 48. Eyre, B. D. Regional evaluation of nutrient transformation and phytoplankton growth in nine river-dominated sub-tropical east Australian estuaries. *Mar. Ecol. Prog. Ser.* **205**, 61–83 (2000).
 49. Eyre, B. D. & Pont, D. Intra- and inter-annual variability in the different forms of diffuse nitrogen and phosphorus delivered to seven sub-tropical east Australian estuaries. *Estuar. Coast. Shelf Sci.* **57**, 137–148 (2003).
 50. Webb, A. P. & Eyre, B. D. Effect of natural populations of burrowing thalassinidean shrimp on sediment irrigation, benthic metabolism, nutrient fluxes and denitrification. *Mar. Ecol. Prog. Ser.* **268**, 205–220 (2004).
 51. SeaTemperature.INFO. *Water Temperature in Yamba*. Vol. 2020. <https://seatemperature.info/yamba-water-temperature.html> (2020).
 52. Greene, R. M., Geider, R. J., Kolber, Z. & Falkowski, P. G. Iron-induced changes in light harvesting and photochemical energy conversion processes in eukaryotic marine algae. *Plant Physiol* **100**, 565–575 (1992).
 53. Mori, T., Binder, B. & Johnson, C. H. Circadian gating of cell division in cyanobacteria growing with average doubling times of less than 24 hours. *Proc. Natl. Acad. Sci. USA.* **93**, 10183 (1996).
 54. Trends in Atmospheric Carbon Dioxide. Vol. 2020. <https://www.esrl.noaa.gov/gmd/ccgg/trends/> (National Oceanic & Atmospheric Administration (NOAA), 2020).
 55. Dickson, A. Standards for ocean measurements. *Oceanography* **23**, 34–47 (2010).
 56. Dickson, A. G., Sabine, C. L. & Christian, J. R. *Guide to Best Practices for Ocean CO₂ Measurements*. (North Pacific Marine Science Organization, 2007).
 57. Simone, M. N., Schulz, K. G., Eyre, B. D. & Oakes, J. M. Ocean acidification may mitigate negative effects of warming on carbon burial potential in subtidal unvegetated estuarine sediments. *Limnol. Oceanogr.* 1–14 <https://doi.org/10.1002/lno.11796> (2021).

58. Ferguson, A. J., Eyre, B. D. & Gay, J. M. Organic matter and benthic metabolism in euphotic sediments along shallow sub-tropical estuaries, northern New South Wales, Australia. *Aquat. Microb. Ecol.* **33**, 137–154 (2003).
59. Ferguson, A. J., Eyre, B. D. & Gay, J. M. Benthic nutrient fluxes in euphotic sediments along shallow sub-tropical estuaries, northern New South Wales, Australia. *Aquat. Microb. Ecol.* **37**, 219–235 (2004).
60. McKee, L., Eyre, B. & Hossain, S. Intra- and interannual export of nitrogen and phosphorus in the subtropical Richmond River catchment. *Australia. Hydrol. Process.* **14**, 1787–1809 (2000).
61. Carvalho, M. C. & Murray, R. H. Osmar, the open-source microsyringe autosampler. *HardwareX* **3**, 10–38 (2018).
62. Nielsen, L. P. Denitrification in sediment determined from nitrogen isotope pairing. *FEMS Microbiol. Ecol.* **9**, 357–361 (1992).
63. Sturm, K. et al. Sampling considerations and assessment of Exetainer usage for measuring dissolved and gaseous methane and nitrous oxide in aquatic systems. *Limnol. Oceanogr. Methods* **13**, 375–390 (2015).
64. Weiss, R. F. & Price, B. A. Nitrous oxide solubility in water and seawater. *Mar. Chem.* **8**, 347–359 (1980).
65. The MathWorks Inc. MATLAB version: 9.5 (R2018b). (The MathWorks Inc., Natick, Massachusetts, 2018).

Acknowledgements

Thanks are extended to P. Kelly, I. Alexander, M. Carvalho, N. Carlson-Perret, J. Yeo, and N. Camillini for their assistance in the field and support in the laboratory. Special thanks to Z. Kennedy for allowing access to their property for sample collection. All listed authors have contributed substantially to the study conception and design and the preparation and drafting of this paper and have approved the final submitted manuscript. The authors declare that they have no conflict of interest. This work was supported in the form of an SESE Postgraduate Scholarship from Southern Cross University, Lismore, NSW, Australia, and ARC Discovery projects DP150102092, DP160100248, and DP2001005546. Datasets for this research are available.

Author contributions

All authors have given approval to the final version of the manuscript. M.S. conceived the project, collected data, ran data analysis and interpretation, and led the writing of the manuscript. D.E. collected data, ran data analysis, and contributed to data interpretation. K.S., J.O., and B.E. conceived the

project and contributed to data interpretation. All authors contributed to writing the manuscript.

Competing interests

The authors declare no competing interests.

Ethics approval

The authors support inclusive, diverse, and equitable conduct of research.

Additional information

Supplementary information The online version contains supplementary material available at <https://doi.org/10.1038/s43247-024-01347-1>.

Correspondence and requests for materials should be addressed to Michelle Nicole Simone.

Peer review information *Communications Earth & Environment* thanks Yanling Zheng and the other, anonymous, reviewer(s) for their contribution to the peer review of this work. Primary handling editors: Olivier Sulpis and Clare Davis. A peer review file is available.

Reprints and permissions information is available at <http://www.nature.com/reprints>

Publisher's note Springer Nature remains neutral with regard to jurisdictional claims in published maps and institutional affiliations.

Open Access This article is licensed under a Creative Commons Attribution 4.0 International License, which permits use, sharing, adaptation, distribution and reproduction in any medium or format, as long as you give appropriate credit to the original author(s) and the source, provide a link to the Creative Commons licence, and indicate if changes were made. The images or other third party material in this article are included in the article's Creative Commons licence, unless indicated otherwise in a credit line to the material. If material is not included in the article's Creative Commons licence and your intended use is not permitted by statutory regulation or exceeds the permitted use, you will need to obtain permission directly from the copyright holder. To view a copy of this licence, visit <http://creativecommons.org/licenses/by/4.0/>.

© The Author(s) 2024